

ORIGINAL RESEARCH

Open Access



Magnetic resonance spectroscopy for enhanced multiparametric MRI characterization of [¹⁸F]FET PET-negative gliomas

Xiaoran Li^{1,2†}, Xinru Xiao^{3†}, Xin Han^{1,2}, Ye Cheng³, Bixiao Cui^{1,2}, Meng Zhang⁴, Huawei Liu⁵ and Jie Lu^{1,2*} 

Abstract

Background Approximately 30–36% of gliomas presented with [¹⁸F]fluoroethyl-L-tyrosine ([¹⁸F]FET) PET-negative at primary diagnosis, which interferes with the differentiation of gliomas from other isolated brain lesions. Preoperative noninvasive identification of [¹⁸F]FET PET-negative gliomas to aggressive surgical treatment could reduce ineffective treatment and improve prognosis. This study aimed to assess the potential utility of multiparametric MRI with ¹H-magnetic resonance spectroscopy (¹H-MRS) in the diagnosis of gliomas within [¹⁸F]FET PET-negative isolated cerebral lesions.

Results A total of 51 patients (mean age 44.35 ± 27.15 years, 26 males) with 37 gliomas and 14 non-gliomas were recruited for the study. More than half of PET-negative gliomas presented T2-FLAIR mismatch sign, whereas non-gliomas were more likely to present absence of T2-FLAIR mismatch sign (54.05% vs. 7.14%, $p < 0.001$). Choline to creatine (Cho/Cr) ratios in gliomas were significantly higher than those in non-gliomas (2.21 vs. 1.30, $p < 0.001$). Multiparametric MRI (AUC = 0.88) outperformed conventional MRI (AUC = 0.72) in differentiating gliomas from non-gliomas (NRI = 0.29, $p = 0.02$). And WHO grade was correlated with Cho/Cr and total lesion tracer standardized uptake (TLU) ($r = 0.43$ and 0.55 ; $p = 0.007$ and < 0.001 ; respectively). Low-grade PET-negative gliomas exhibit low levels of both TLU and Cho/Cr, but the distribution of TLU and Cho/Cr is more variable in high-grade gliomas. Furthermore, there was a moderate correlation between TLU and Cho/Cr in low-grade PET-negative gliomas ($r = 0.54$, $p = 0.017$), whereas there was no correlation in the high-grade PET-negative gliomas ($r = -0.017$, $p = 0.95$).

Conclusion Multiparametric MRI with ¹H-MRS demonstrates significant promise in enhancing the diagnosis and overall clinical management for [¹⁸F]FET PET-negative gliomas. Moreover, the correlation between TLU and Cho/Cr that was affected by tumor grading of 2021 WHO criteria provides a rationale for further research into the mechanisms of reduced [¹⁸F]FET uptake in gliomas.

Keywords Gliomas, [¹⁸F]FET, PET/MR, PET-negative, Multiparametric MRI

[†]Xiaoran Li and Xinru Xiao have contributed equally to this work.

*Correspondence:

Jie Lu

Imaginglu@hotmail.com

Full list of author information is available at the end of the article

Background

Preoperative non-invasive identification of gliomas has been a challenge and a crucial factor in glioma-related clinical treatment decisions. Positron emission tomography (PET) with radiolabeled amino acids including [^{18}F] fluoroethyl-L-tyrosine ([^{18}F]FET) tracer play an important role in localizing tumor lesions for biopsy, differential diagnosis, and recurrence determination due to the specific uptake of amino acid tracers by tumor cells [1–3]. [^{18}F]FET PET imaging performed well in differentiating primary high-grade and low-grade gliomas (accuracy, 70.4–75%) [4, 5]. However, 30–36% of gliomas may interfere with the diagnosis due to [^{18}F]FET PET-negative findings [2].

[^{18}F]FET PET-negative cerebral lesions suspicious for gliomas mainly composed of demyelination, metastasis, lymphomas, and a small proportion of gliomas [2]. But the surgical resection is the necessity for clinical treatment of gliomas, which is distinct from the treatment of other lesions. And PET-negative gliomas performed a significantly prolonged progression free survival as compared to PET-positive glioma patients (23.1 ± 16.7 m vs. 16.4 ± 14.2 m; $p = 0.003$) [6]. Therefore, preoperative non-invasive identification of [^{18}F]FET PET-negative gliomas to aggressive surgical treatment could reduce ineffective treatment and improve patient prognosis. However, inexperienced nuclear medicine doctors relying on PET imaging alone have difficulty definitively diagnosing [^{18}F]FET PET-negative gliomas.

In contrast, multiparametric MRI integrating conventional and advanced MRI has been used for multi-dimensional assessment of gliomas preoperatively and postoperatively [7]. The T2-FLAIR mismatch sign based on conventional MRI was an imaging biomarker for the specific identification of IDH-mutant with 1p/19q non-codeleted (IDHmut-Noncodelet) astrocytoma in lower grade gliomas, but its sensitivity was only 22–46% [8, 9]. However, the value of lesion location, enhancement, necrosis, and edema in distinguishing gliomas from other cerebral lesions remained contentious across various studies [10–12]. The utilization of advanced MRI, including magnetic resonance spectroscopy (MRS), diffusion-weighted imaging (DWI), and arterial spin labeling (ASL) imaging, facilitated the quantitative identification of gliomas in contrast to conventional MRI [13]. The minimal apparent diffusion coefficient (ADC_{min}) exhibited a significant elevation in tumefactive demyelinating lesions compared to high-grade gliomas [10]. MRS revealing the molecular composition of a specific tissue provided a distinctive understanding of the physiological or pathophysiological mechanisms underlying gliomas [14, 15]. Gliomas with enhanced infiltrative and invasive characteristics likely demonstrated increased

choline to creatine (Cho/Cr) and choline to acetylaspartate (Cho/NAA) ratios [16, 17]. Malignant tumor lesions stimulate the neoangiogenesis in the brain, leading to an increase in cerebral blood perfusion (CBF), which forms the basis for utilizing ASL imaging to distinguish gliomas from other non-neoplastic lesions [18]. Moreover, several studies have demonstrated the higher precision of multiparametric MRI in identifying gliomas from other types of lesions than single parameter MRI [19, 20]. Therefore, we hypothesized that the application of multiparametric MRI could enhance diagnosing gliomas in [^{18}F]FET PET-negative isolated cerebral lesions.

With the clinical application of hybrid PET/MR scanners in gliomas, exploring how to efficiently apply multimodal imaging to improve diagnostic accuracy is a research hotspot. Currently, some [^{18}F]FET PET/MRI studies have focused on the preoperative diagnosis and tumor localization of gliomas [21–23]. The combination of [^{18}F]FET PET and MRS could be used to differentiate glioblastoma from non-glioblastoma [24]. However, the additional and potential values of hybrid multiparametric MRI in the PET/MRI scanning for the preoperative diagnosis of gliomas in [^{18}F]FET PET-negative isolated cerebral lesions remain not investigated. We aimed to underscore the potential value of multiparametric MRI in identifying gliomas with [^{18}F]FET PET-negative findings to offer valuable surgical guidance and enhance the overall clinical management of these [^{18}F]FET PET-negative challenging cases.

Methods

Study design and patients

Between March 2023 and May 2024, participants with isolated cerebral lesions who initially suspected gliomas based on conventional MRI at the Xuanwu hospital were prospectively enrolled. All patients underwent a brain multi-parametric [^{18}F]FET PET/MR scan followed by biopsy or lesion resection surgery. Inclusion criteria included (1) age greater than 18 years, (2) no absolute contraindications to PET/MR examination, (3) conventional brain MRI initial suspicion of gliomas by one radiologist with more than 7 years of experience in the diagnosis of neuro-oncology and one neuro-oncologist with more than 20 years of experience, and (4) cerebral lesions showed a [^{18}F]FET PET-negative presentation that the maximal tumor to background ratio (TBR_{max}) on PET images was less than 1.6 or absence of any visually increased signal abnormality in PET imaging according to PET imaging guidelines for gliomas [1, 2]. A participant was excluded if he or she met any of the subsequent criteria: (1) incomplete or poor-quality PET/MR images, (2) with malignant brain tumors of non-neuroepithelial origin diagnosed by pathology, (3) no surgical treatment

or biopsy to acquire pathologic evidence, and (4) absence of 2021 World Health Organization (WHO) classification of tumors of the central nervous system taxonomy. Flow chart of inclusion and exclusion is shown in Fig. 1.

Pathology

Pathology analysis of lesions was defined at surgery or biopsy performed by two pathologists with more than 10-year neuro-oncology pathological diagnosis in a blinded manner according to the 2021 WHO classification of brain tumors. Hematoxylin–eosin (H&E) and Ki-67 (ZSGB-BIO, Beijing, China, mouse monoclonal, diluted 1:50) immunohistochemistry with diaminobenzidine staining (Polink-1HRP Broad Spectrum DAB Detection Kit, Golden Bridge International, Mukilteo, USA)

were used to initially evaluate the cell proliferative index of lesions for determining gliomas. The subsequent IDH mutation and chromosome 1p/19q co-deletion were identified by the whole-exome next-generation sequencing for classifying the glioma molecular type. Luxol fast blue (LFB) and H&E staining were performed to further validate demyelination for highly suspected demyelinating lesions. All images of section were captured with Leica Biosystems (Leica Aperio AT Turbo, USA).

PET/MR imaging

All [¹⁸F]FET PET/MR images were acquired with a 3.0T integrated PET/MRI (GE Healthcare) scanner using 19-channel head-neck coil. All patients adhered to a minimum fasting period of 4 h, followed by brain

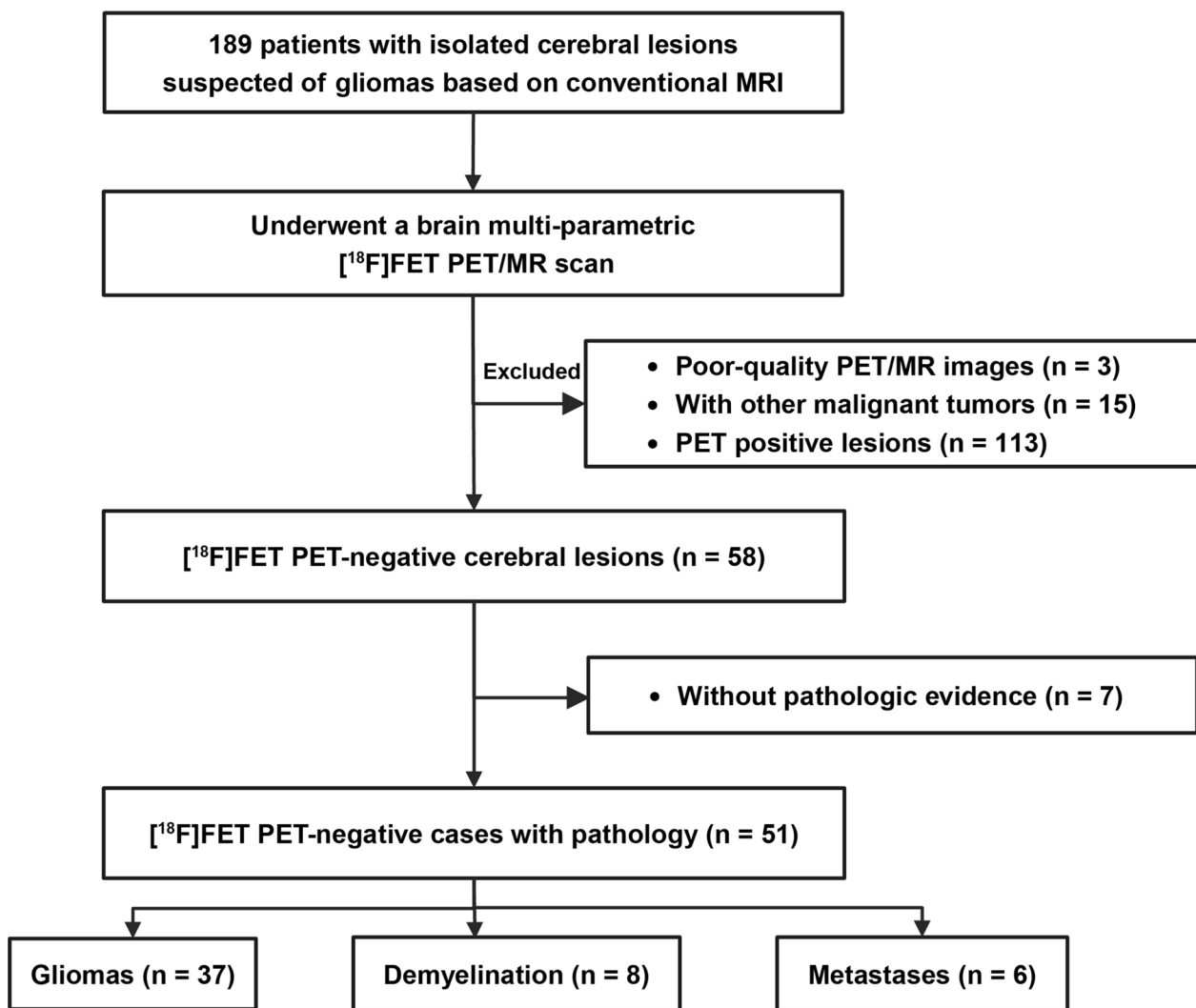


Fig. 1 The flowchart of enrolled and excluded criteria. 189 patients suspected of gliomas were initially recruited to perform a brain [¹⁸F]FET PET/MR scanning. A total of 51 cases of [¹⁸F]FET PET-negative isolated cerebral lesions were enrolled after excluding 25 cases

simultaneously MRI and PET scanning within a time frame of 20–40 min after the 185–200 MBq [¹⁸F]FET injection. The MR imaging sequences for the brain comprised 3D T1 weighted imaging (T1WI), axial T2 weighted imaging (T2WI), axial T2 fluid attenuated inversion recovery (T2-FLAIR), DWI, 3D ASL, 2D multivoxel ¹H-MRS, and an 3D T1 contrast enhanced (T1CE) sequence. MRS scans were localized at the maximum cross section of the lesion with enhancement on the T1CE images or absolute intensity maximum on T2-FLAIR images, and avoided contamination by normal cerebral tissue, the skull base, hemorrhage, and the ventricular system. And the MRS pre-scan data was required to achieve full width at half maximum less than 0.096 ppm and percentage standard deviation (SD) less than 20% before formal scanning. The PET images were acquired in 3D mode with an axial field-of-view of 35 cm. An 18-s 2-point Dixon scan was acquired for MRI-based PET attenuation correction. And brain attenuation-corrected PET images were reconstructed by using the ordered subset expectation maximization algorithm (6 iterations, 16 subsets, and full width at half maximum of a Gaussian filter of 3.0 mm) under the time-of-flight technique with a 256×256 matrix and 2.78 mm slice thickness. Detailed scanning settings and parameters of PET/MRI sequences were summarized in Supplementary Table S1.

Imaging analysis

All PET/MR images were loaded into image processing workstation (AW4.7, GE Healthcare) to perform imaging analysis. ADC and CBF maps were respectively obtained from DWI and ASL imaging using workstation. Then PET, T2, T2-FLAIR, ADC, and CBF images were registered to the 3D T1 image with a 1 mm isovoxel, respectively. Since all cerebral lesions showed [¹⁸F]FET PET-negative (TBR < 1.6), the definition of volume of interests (VOI) of tumors was defined by two neuroradiologists manually contouring the abnormal high intensity area on T2-FLAIR or enhanced signal area on T1CE, avoiding necrosis, calcification, cysts, and hemorrhage (Supplementary Fig. 1) [1, 2, 25]. The maximum standardized uptake value (SUV_{max}), mean SUV (SUV_{mean}), TBR_{max}, TBR_{mean}, tumor volume (TV), and total lesion tracer standardized uptake (TLU = TV × SUV_{mean}) based on VOI were calculated for evaluating [¹⁸F]FET uptake.

Conventional MRI analysis consisted of lesion location, T2-FLAIR mismatch sign, hemorrhage, edema, necrosis, and enhancement. ADC_{min} and CBF_{max} were calculated from ADC and CBF images based on VOI. A circular (diameter 50 mm) was drawn in the normal cerebral hemisphere at the slice of the centrum semiovale including cortical and white matter for calculating the

parameters of background cerebral tissue to acquire the relative ADC_{min} (rADC_{min}) and relative CBF_{max} (rCBF_{max}) [26]. Compound metabolism data of ¹H-MRS data were generated by workstation, providing automatic baseline correction, peak assignment, and ratio calculation. Metabolic measurements were performed by selecting 3–5 voxels to calculate the mean metabolic value from the voxels that were not significantly distorted baselines and located at the site with enhancement in T1CE or with high signal in T2 FLAIR images. The voxels containing normal cerebral tissue, the skull base, hemorrhage, and the ventricular system were excluded to calculate. The signal intensities were calculated by the sum of each peak, and relative ratios were calculated by the division of two concentrations. The noise level was defined as the variation of noise region (range 0.4–0.9 ppm). To avoid spuriously high-ratio values, voxels were excluded if the signal to noise ratio (SNR) of Cr was less than 3. In addition to recording the peak area ratios of Cho/Cr and Cho/NAA, the myo-inositol (MI) peaks and the lactate-lipid (LL) peaks were recorded in four levels (undetectable, positive and detectable, strongly positive, and extremely strongly positive) as described in previous study [27].

Statistical analysis

The distribution of conventional and advanced MRI parameters between gliomas and non-gliomas group were analyzed by Chi-square test or Mann–Whitney U test/t-test. Furthermore, post-hoc multiple comparisons based on the Kruskal–Wallis test were used to compare differences in advanced MRI parameters among gliomas, demyelination, and metastasis. The MRI variables for which statistical significance existed for the above tests were continued to be used in univariate and multivariate logistic regression analyses to predict gliomas from all lesions. Receiver operating characteristic curve (ROC) and decision curve analysis (DCA) were used to evaluate the accuracy and clinical value of conventional and multiparametric MRI predicting gliomas. Besides, net reclassification improvement (NRI) was calculated to compare the difference in diagnostic efficacy for gliomas between conventional and multiparametric MRI. The correlation between MRI parameters and WHO grades was investigated by paired Spearman's tests.

All statistical analyses were conducted by using R software (version 4.3.1, Vienna, Austria) and python (version 3.7). A *p* value < 0.05 was regarded as statistically significant.

Results

Demographics of patients

Fifty-one patients (44.35 ± 27.15 years old, 26 males and 25 females) with [¹⁸F]FET PET-negative primary isolated

Table 1 Demographics of enrolled patients

Variable	All patients (n = 51)
Age, years	44.35 ± 27.15
Sex	
Female	25 (49.02%)
Male	26 (50.98%)
Pathology	
Gliomas	37 (72.55%)
Non-gliomas	14 (27.45%)
2021 WHO grade	
WHO grade 1	2 (5.41%)
WHO grade 2	17 (45.94%)
WHO grade 3	5 (13.51%)
WHO grade 4	13 (35.14%)
TBR _{max}	1.35 ± 0.28
SUV _{max}	1.80 ± 0.65

Data were described as mean ± SD or numbers (%). SD indicates standard deviation

cerebral lesions were prospectively included following excluding 25 cases (Fig. 1). There were 37 gliomas and 14 non-gliomas (8 demyelination cases and 6 brain metastases cases, Table 1). 19 PET-negative cases with WHO 1–2 grade gliomas were grouped as low-grade gliomas, and 18 PET-negative cases with WHO 3–4 grade gliomas were classified as high-grade gliomas (Table 1).

Conventional MRI characteristics

Conventional MRI features distribution between gliomas group and non-gliomas group are summarized in the Table 2. There was a significant difference in proportion of T2-FLAIR mismatch sign between the gliomas and non-gliomas ($p < 0.001$). More than half of PET-negative gliomas (54.05%) presented T2-FLAIR mismatch sign, whereas non-gliomas were more likely to present absence of T2-FLAIR mismatch sign (94.44%). No significant differences of lesion location, enhancement, hemorrhage, edema, and necrosis were revealed between gliomas and non-gliomas ($p = 0.806, 0.478, 0.753, 0.196,$ and 0.191 , respectively; Table 2). Figure 2 illustrates the PET and conventional MRI findings of [¹⁸F]FET negative cases.

Advanced MRI parameters

The ADC_{min} (661.86 ± 199.63 vs. $598.50 \pm 147.55 \times 10^{-6}$ mm²/s, $p = 0.294$) and rADC_{min} (1.15 ± 0.36 vs. 1.01 ± 0.35 , $p = 0.258$) were not different between PET-negative gliomas and non-gliomas (Table 3). And no significant differences were observed in CBF_{max}, rCBF_{max}, CBF_{mean}, and rCBF_{mean} between gliomas and non-gliomas (all $p > 0.05$, Table 3). The Cho/NAA ratio (2.25 vs. 1.10 , $p < 0.001$) and Cho/Cr ratio (2.21 vs. 1.30 , $p < 0.001$) of gliomas were

Table 2 Conventional MRI parameters of gliomas and non-gliomas

Features	All types (n = 51)	Non-gliomas (n = 14)	Gliomas (n = 37)	χ ²	p
Location				2.29	0.806*
Frontal	23 (45.10%)	6 (42.86%)	17 (45.95%)		
Temporal	10 (19.61%)	2 (14.29%)	8 (21.62%)		
Parietal	2 (3.92%)	0 (0.00%)	2 (5.41%)		
Occipital	4 (7.84%)	1 (7.14%)	3 (8.11%)		
Insular	7 (13.73%)	3 (21.43%)	4 (10.81%)		
Others	5 (9.80%)	2 (14.29%)	3 (8.11%)		
T2-FLAIR mismatch				9.23	0.003*
Absent	30 (58.82%)	13 (92.86%)	17 (45.95%)		
Present	21 (41.18%)	1 (7.14%)	20 (54.05%)		
Hemorrhage				0.53	0.478*
Absent	49 (96.08%)	13 (92.86%)	36 (97.30%)		
Present	2 (3.92%)	1 (7.14%)	1 (2.70%)		
Edema				0.10	0.753
Absent	20 (39.22%)	5 (35.71%)	15 (40.54%)		
Present	31 (60.78%)	9 (64.29%)	22 (59.46%)		
Necrosis				1.67	0.196
Absent	29 (56.86%)	10 (71.43%)	19 (51.35%)		
Present	22 (43.14%)	4 (28.57%)	18 (48.65%)		
Enhancement				3.31	0.191
Absent	24 (47.06%)	4 (28.57%)	20 (54.05%)		
Rim	16 (31.37%)	5 (35.71%)	11 (29.73%)		
Patchy	11 (21.57%)	5 (35.71%)	6 (16.22%)		

Data were described as numbers (%). *Represented fisher’s exact correction for chi-square test

significantly higher than those of non-gliomas (Table 3). But there was no difference in MI and LL levels between gliomas and non-gliomas (Table 3). Moreover, multiple comparisons showed the Cho/NAA ratio of gliomas were higher than that of metastases ($p = 0.007$), but the difference in Cho/NAA ratio between gliomas and demyelination was not observed ($p = 0.103$; Fig. 3). And the Cho/Cr ratio of gliomas was higher than that of metastases and demyelination ($p < 0.001$, respectively; Fig. 3). The advanced MRI findings of [¹⁸F]FET negative cases are demonstrated in Fig. 4.

Performance for identifying PET-negative gliomas

Both the univariate and multivariate logistic regression analyses revealed that T2-FLAIR mismatch and Cho/Cr were significantly associated with gliomas ($p < 0.05$). The Odds Ratio (OR) values and detailed p values of MRI parameters in logistic regression for predicting gliomas are described in the Table 4. Thus, nomogram integrating T2-FLAIR mismatch and Cho/Cr was established by logistic regression for predicting gliomas from PET-negative lesions (Fig. 5A). ROC analysis showed that

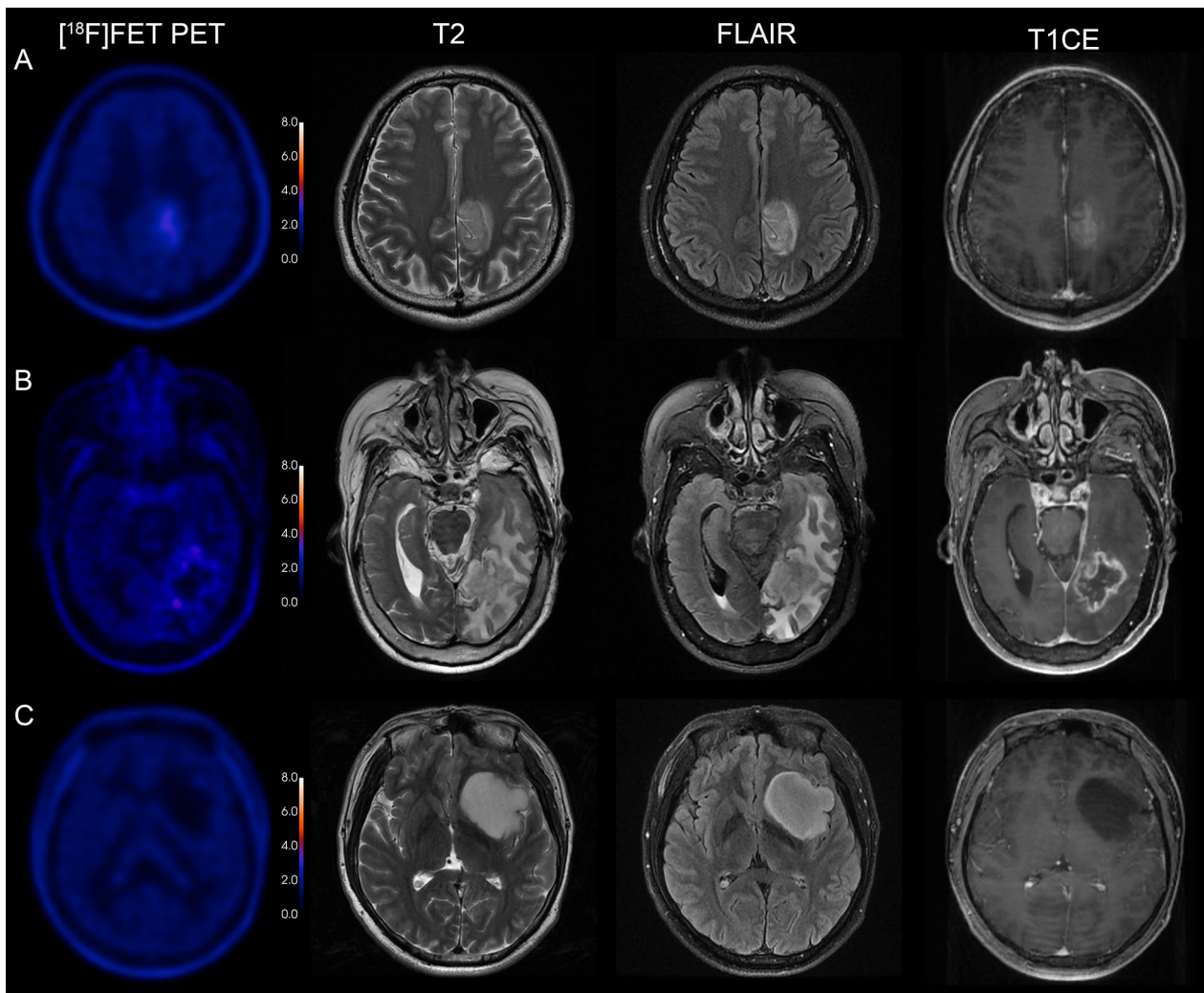


Fig. 2 PET and conventional MRI of $[^{18}\text{F}]$ FET PET-negative lesions. **A** A 55-year-old male with demyelination lesion. Conventional MRI showed patch enhancement isolated lesion located in the left central zone with negative $[^{18}\text{F}]$ FET uptake ($\text{TBR}_{\text{max}} = 1.56$). **B** A 46-year-old female with brain metastasis pulmonary adenocarcinoma proven by histopathology. Conventional MR images showed rim enhancement isolated lesion located in the left occipital lobe with negative $[^{18}\text{F}]$ FET uptake ($\text{TBR}_{\text{max}} = 1.35$). **C** A 29-year-old male with astrocytoma, WHO grade 2. Conventional MR images showed non enhancement isolated lesion located in the left insula lobe with negative $[^{18}\text{F}]$ FET uptake ($\text{TBR}_{\text{max}} = 1.07$). TBR_{max} indicates maximal tumor to background ratio

AUC value of nomogram based on multiparametric MRI ($\text{AUC} = 0.88$) was greater than that of conventional MRI ($\text{AUC} = 0.73$; Fig. 5B). The accuracy of multiparametric MRI in differentiating gliomas and non-gliomas was 92%, with a sensitivity of 97% and a specificity of 79% (Table 5).

Besides, the decision curve analysis indicated that the nomogram based on multiparametric MRI has a better net benefit of screening than the conventional MRI (Fig. 5C). The confusion matrix revealed that 4 cases were mistakenly classified by the multiparametric MRI nomogram in detecting PET-negative gliomas, as shown in the green on-diagonal entries of the confusion matrix (Fig. 5D). The NRI analysis showed a 29% improvement

in the ability of multiparametric MRI to discriminate gliomas from non-gliomas in PET-negative lesions compared to conventional MRI ($p = 0.02$; Supplementary Table S2).

Advanced MRI characterization of PET-negative gliomas

Heatmap of Z-score showed that high-grade (WHO 3–4) PET-negative gliomas had higher Cho/NAA, Cho/Cr, and TLU than those of low-grade (WHO 1–2) gliomas (Fig. 6A). And WHO grade was correlated with Cho/Cr and TLU ($r = 0.43$ and 0.55 ; $p = 0.007$ and < 0.001 ; respectively; Fig. 6B). Simultaneously, there was a correlation between Cho/Cr and TLU ($r = 0.33$, $p = 0.042$), as shown

Table 3 Advanced MRI parameters of gliomas and non-gliomas

Advanced MRI parameters	Non-gliomas (n = 14)	Gliomas (n = 37)	t/Z/ χ^2	p
ADC _{min} , 10 ⁻⁶ mm ² /s	598.50 ± 147.55	661.86 ± 199.63	- 1.06	0.294
ADC _{mean} , 10 ⁻⁶ mm ² /s	1162.30 ± 283.35	1217.81 ± 217.46	- 0.73	0.469
rADC _{min}	1.01 ± 0.35	1.15 ± 0.36	- 1.14	0.258
rADC _{mean}	1.29 ± 0.33	1.44 ± 0.29	- 1.56	0.125
CBF _{max} , ml/100 g/min	58.00 [53.00,96.00]	70.00 [58.00,86.00]	- 0.40	0.696
CBF _{mean} , ml/100 g/min	29.22 [22.98,36.12]	38.09 [33.14,44.20]	- 1.90	0.059
rCBF _{max}	1.19 [0.92,1.53]	1.00 [0.81,1.24]	1.73	0.085
rCBF _{mean}	0.92 [0.77,1.19]	0.89 [0.71,1.08]	1.16	0.250
Cho/NAA	1.10 [0.76,1.63]	2.25 [1.71,3.70]	- 3.32	<0.001
Cho/Cr	1.30 [1.21,1.50]	2.21 [1.91,3.03]	- 4.00	<0.001
MI			2.09	0.350
(-)	14 (30.43%)	32 (69.57%)		
(+)	0 (0.00%)	4 (100.00%)		
(++)	0 (0.00%)	1 (100.00%)		
LL			5.23	0.155
(-)	9 (29.03%)	22 (70.97%)		
(+)	5 (45.45%)	6 (54.55%)		
(++)	0 (0.00%)	7 (100.00%)		
(+++)	0 (0.00%)	2 (100.00%)		

Dates were described as mean ± SD/median [IQR] or numbers (%). ADC indicates apparent diffusion coefficient; CBF, cerebral blood perfusion; Cho/Cr, choline to creatine; Cho/NAA, choline to acetylaspertate; LL, lactate-lipid; MI, myo-inositol; rADC, relative apparent diffusion coefficient; rCBF, relative cerebral blood perfusion

in Fig. 6B. But distribution of TLU and Cho/Cr were different between high-grade gliomas and low-grade gliomas (Fig. 6C). Low-grade PET-negative gliomas exhibit low levels of both TLU and Cho/Cr, but the distribution of TLU and Cho/Cr is more variable in high-grade gliomas (Fig. 6C). Furthermore, there was a moderated correlation between TLU and Cho/Cr in low-grade PET-negative gliomas ($r=0.54$, $p=0.017$; Fig. 6D), whereas there was no correlation in the high-grade PET-negative gliomas ($r=-0.017$, $p=0.95$; Fig. 6E).

Discussion

[¹⁸F]FET PET is a highly valuable clinical examination recognized by neurooncologists for the detection of gliomas. However, the identification of [¹⁸F]FET PET-negative gliomas represents a significant challenge for clinics, particularly in the situation where a glioma is suspected by conventional MRI. This study using an integrated PET/MR scanner analyzed the multiparametric MRI manifestations of common [¹⁸F]FET PET-negative isolated cerebral lesions and explored the combination of MRI parameters that can identify gliomas from other negative lesions. For the conventional MRI analysis, only the T2-FLAIR mismatch sign could distinguish gliomas from other PET-negative isolated cerebral lesions. Moreover, the Cho/NAA ratio and Cho/Cr ratio of gliomas were significantly higher than those of non-gliomas.

Thus, a combination of T2-FLAIR mismatch and Cho/Cr performed better in identifying [¹⁸F]FET PET-negative gliomas. The correlation between Cho/Cr and TLU is noteworthy because it was different between high-grade and low-grade gliomas. This result has further strengthened our hypothesis that the metabolite of MRS is a potential tool for providing additional value for identifying [¹⁸F]FET PET-negative gliomas.

Differential distribution of T2-FLAIR mismatch between gliomas and non-gliomas may be attributed to the high proportion of astrocytomas among the PET-negative gliomas, and other studies have confirmed that the T2-FLAIR mismatch sign could diagnose lower-grade astrocytomas with a specificity of over 90% [2, 9]. Previous studies have reported that astrocytomas constitute approximately 73–77% of [¹⁸F]FET PET-negative gliomas [6, 25, 28]. But in this study, the proportion of astrocytomas among PET-negative gliomas was found to be approximately 46% (17/37). The reason for this is that the 2021 WHO typing criteria were utilized instead of the 2016 WHO typing criteria in this research, resulting in the reclassification of some astrocytomas previously categorized based on the 2016 WHO criteria [29]. These reclassified astrocytomas are now identified as IDH wild-type glioblastomas (WHO grade 4) due to the lack of IDH mutations. Hiremath et al. [30] also found that the T2-FLAIR mismatch sign showed a statistically

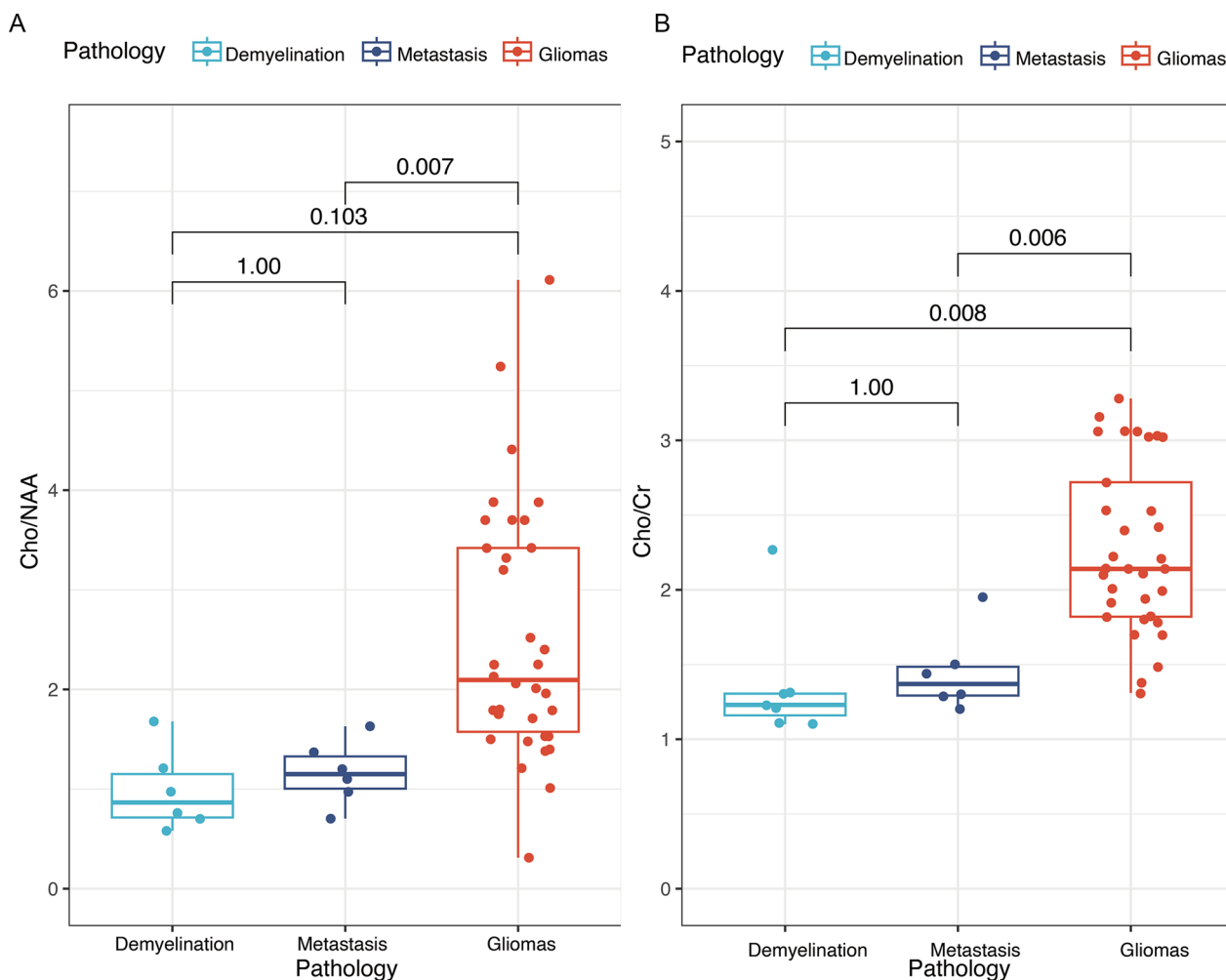


Fig. 3 The distribution of Cho/NAA and Cho/Cr in the PET-negative lesions. **A** The pairwise comparisons of Cho/NAA showed that PET-negative gliomas had higher Cho/NAA than those of demyelination and metastasis. **B** The pairwise comparisons of Cho/Cr showed that both metastasis and gliomas had higher Cho/Cr than that of demyelination. Cho/Cr indicates choline to creatine; Cho/NAA, choline to acetylaspertate

significant difference between demyelination and gliomas. Moreover, a recent search found that the T2-FLAIR mismatch sign in adult-type diffuse glioma lacking contrast enhancement demonstrated 100% specificity and 100% positive predictive value for the IDH mutation, and the absence of the T2-FLAIR mismatch sign (OR=4.71, $p=0.008$) was associated with 1p/19q codeletion [31]. This also indirectly supports our observations, which showed that 47.06% of PET-negative gliomas performed absence of contrast enhancement. Thus, the T2-FLAIR mismatch sign can help identify PET-negative gliomas and is a reliable conventional MRI biomarker for the diagnosis of PET-negative astrocytomas.

Some studies also found that other conventional MRI visual features could not discriminate gliomas from other non-glioma lesions [32, 33]. The reason for this is that gliomas, demyelination, and metastasis can present similar

enhancement, edema, and necrosis in conventional MRI. Our study similarly demonstrated that lesion location, hemorrhage, edema, necrosis, and enhancement could not provide additional values for identifying $[^{18}\text{F}]\text{FET}$ PET-negative gliomas.

In accordance with the present results, previous studies have demonstrated that advanced MRI parameters could be used to differentiate gliomas from other non-glioma lesions [18–20, 34, 35]. Caravan et al. [34] found that ADC_{min} of high-grade gliomas were higher than those in brain metastasis. But in our study, the difference in ADC_{min} between gliomas and non-gliomas was not significant may be due to two factors. Firstly, our study focused on $[^{18}\text{F}]\text{FET}$ PET-negative gliomas, which exhibited lower tumor cell density activity compared to PET-positive gliomas. The results of some studies that confirmed that metabolic parameters of the amino acid

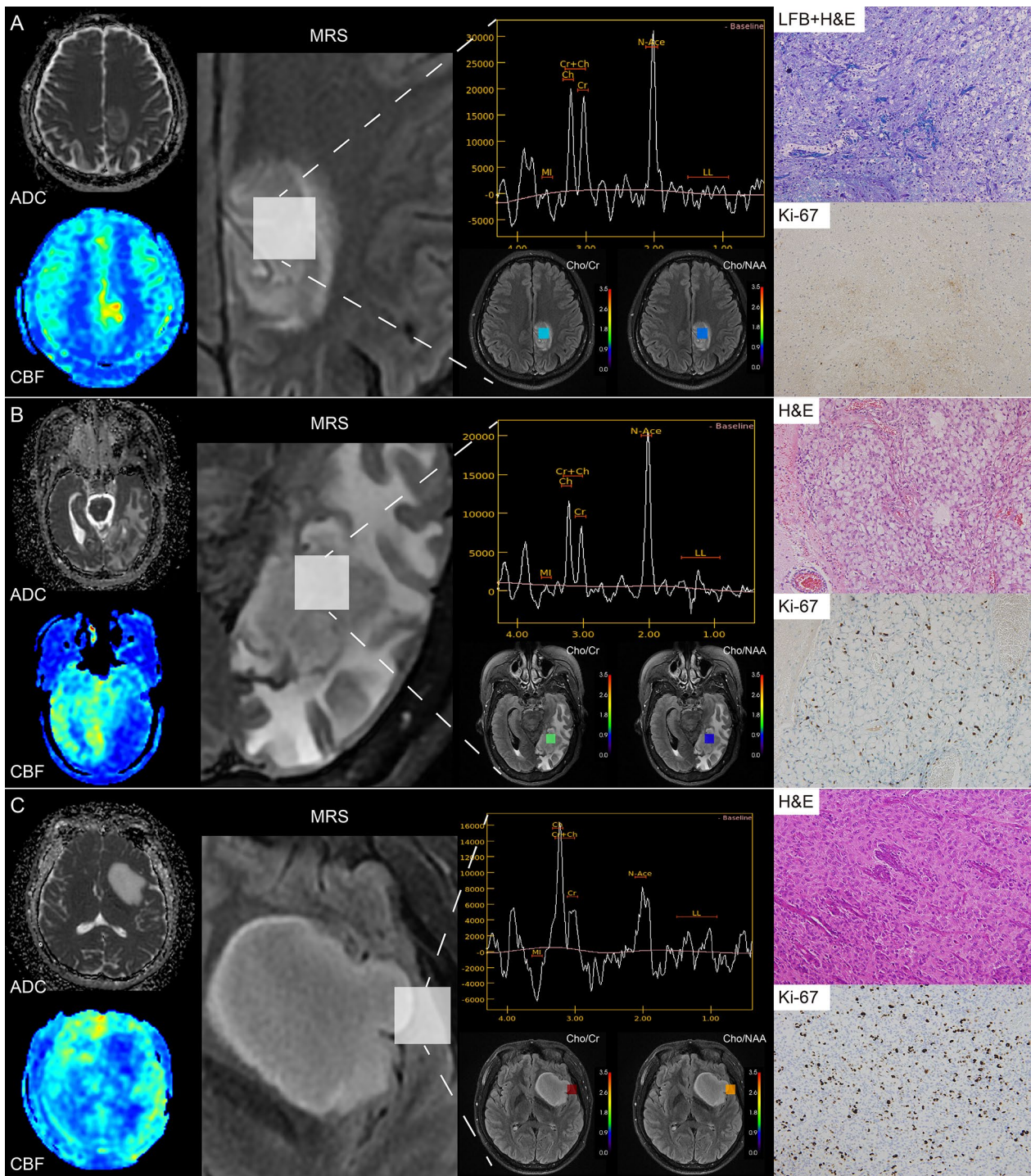


Fig. 4 Advanced MRI and pathology of [^{18}F]FET PET-negative lesions. **A** A 55-year-old male with demyelination lesion. Advanced MRI showed lower diffusion ($rADC_{min} = 0.92$), mild-to-moderate increase of CBF ($rCBF_{max} = 1.52$), lower metabolism (Cho/Cr = 1.21 and Cho/NAA = 0.75). The demyelination with low Ki-67 expression was identified by the LFB and H&E staining ($\times 200$). **B** A 46-year-old female with brain metastasis derived from pulmonary adenocarcinoma. Advanced MRI showed mild diffusion ($rADC_{min} = 1.19$), lower CBF ($rCBF_{max} = 0.72$), lower metabolism (Cho/Cr = 1.29 and Cho/NAA = 0.67). The Ki-67 index was 0.08 ($\times 400$). **C** A 29-year-old male with astrocytoma, WHO grade 3. Advanced MRI showed mild diffusion ($rADC_{min} = 1.10$), lower CBF ($rCBF_{max} = 0.84$), markedly higher metabolism (Cho/Cr = 2.52 and Cho/NAA = 2.12). The tumor tissue had moderate proliferative activity (Ki-67 = 0.10, $\times 400$). ADC_{min} indicates minimal apparent diffusion coefficient; CBF, cerebral blood perfusion; Cho/Cr, choline to creatine; Cho/NAA, choline to acetylaspartate; $rCBF_{max}$, relative maximum cerebral blood perfusion

Table 4 Univariate and multivariate analysis for predicting gliomas

Variables	Univariate analysis			Multivariate analysis		
	OR	95%CI	p	OR	95%CI	p
T2-FLAIR mismatch	15.29	2.63–292.41	0.01	10.99	1.32–91.41	0.03
Cho/NAA	1.23	0.97–1.95	0.25	–	–	–
Cho/Cr	4.8	1.53–21.01	0.02	1.28	0.96–1.71	0.10

Cho/Cr indicates choline to creatine; Cho/NAA, choline to acetylaspartate; CI, confidence interval; OR, odds ratio

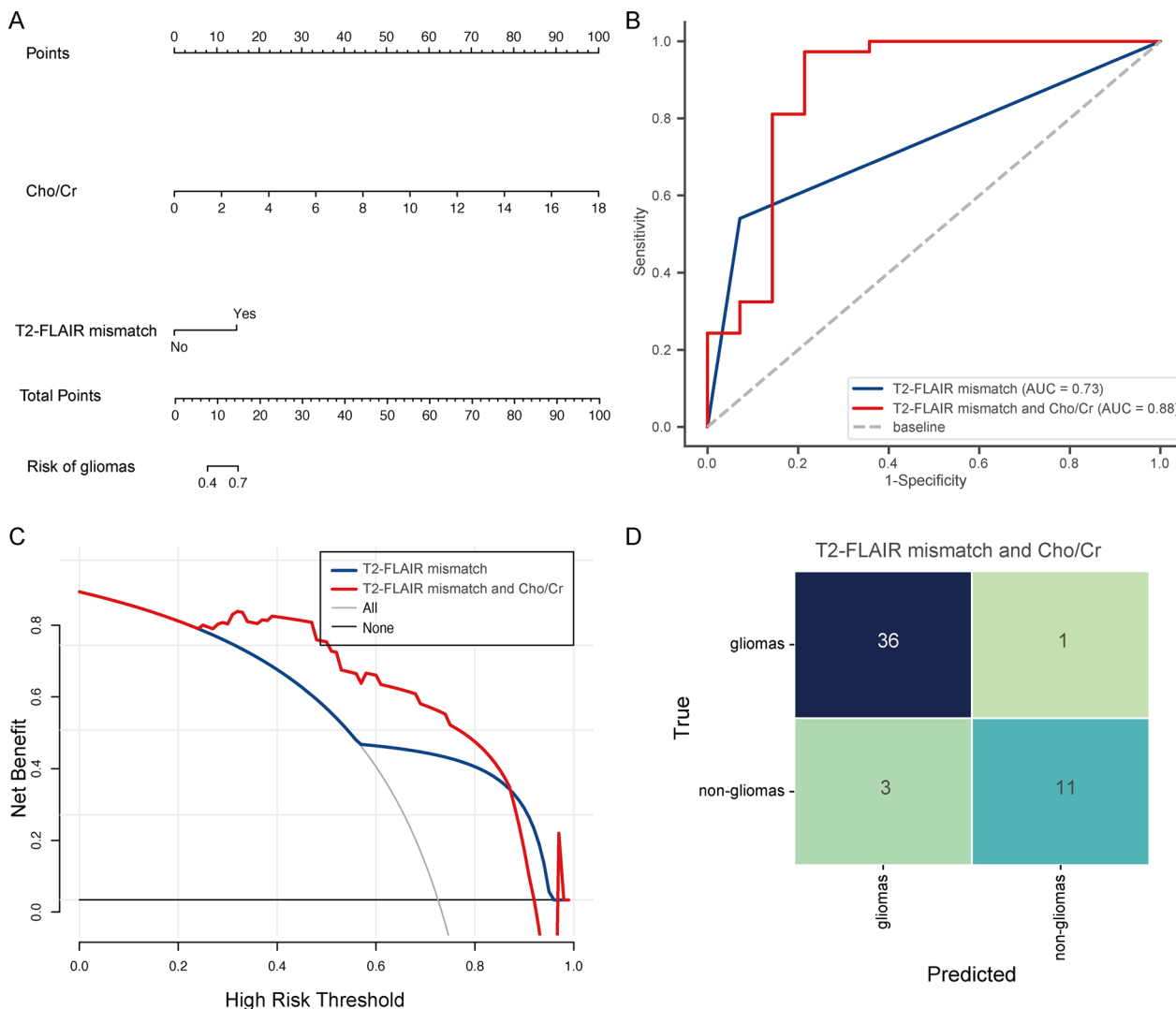


Fig. 5 Nomogram and performance of multiparametric MRI for predicting gliomas. **A** Multi-parametric MRI nomogram integrating conventional MRI and MRS for predicting gliomas in PET-negative isolated cerebral lesions. **B** ROC curves of conventional and multi-parametric MRI nomogram. **C** DCA curves based on conventional and multi-parametric MRI nomogram. **D** Confusion matrix of multi-parametric MRI nomogram for predicting [¹⁸F]FET PET-negative gliomas. AUC, area under the receiver operating characteristic curve; DCA indicates decision curve analysis; ROC, receiver operating characteristic curve

PET are correlated with tumor cell proliferation activity in gliomas supported our hypothesis [36]. Secondly, the gliomas in this study included all grades of gliomas

according to the 2021 WHO grading criteria, which is different from the previous studies that only focused on the high-grade gliomas. Furthermore, the correlation

Table 5 ROC analysis for predicting gliomas

Model	AUC (95%CI)	Sensitivity	Specificity	Accuracy	Youden index
Conventional	0.73 (0.63–0.84)	0.54	0.93	0.65	0.47
Multi-parametric	0.88 (0.75–1.00)	0.97	0.79	0.92	0.76

AUC indicates area under the receiver operating characteristic curve; CI, confidence interval

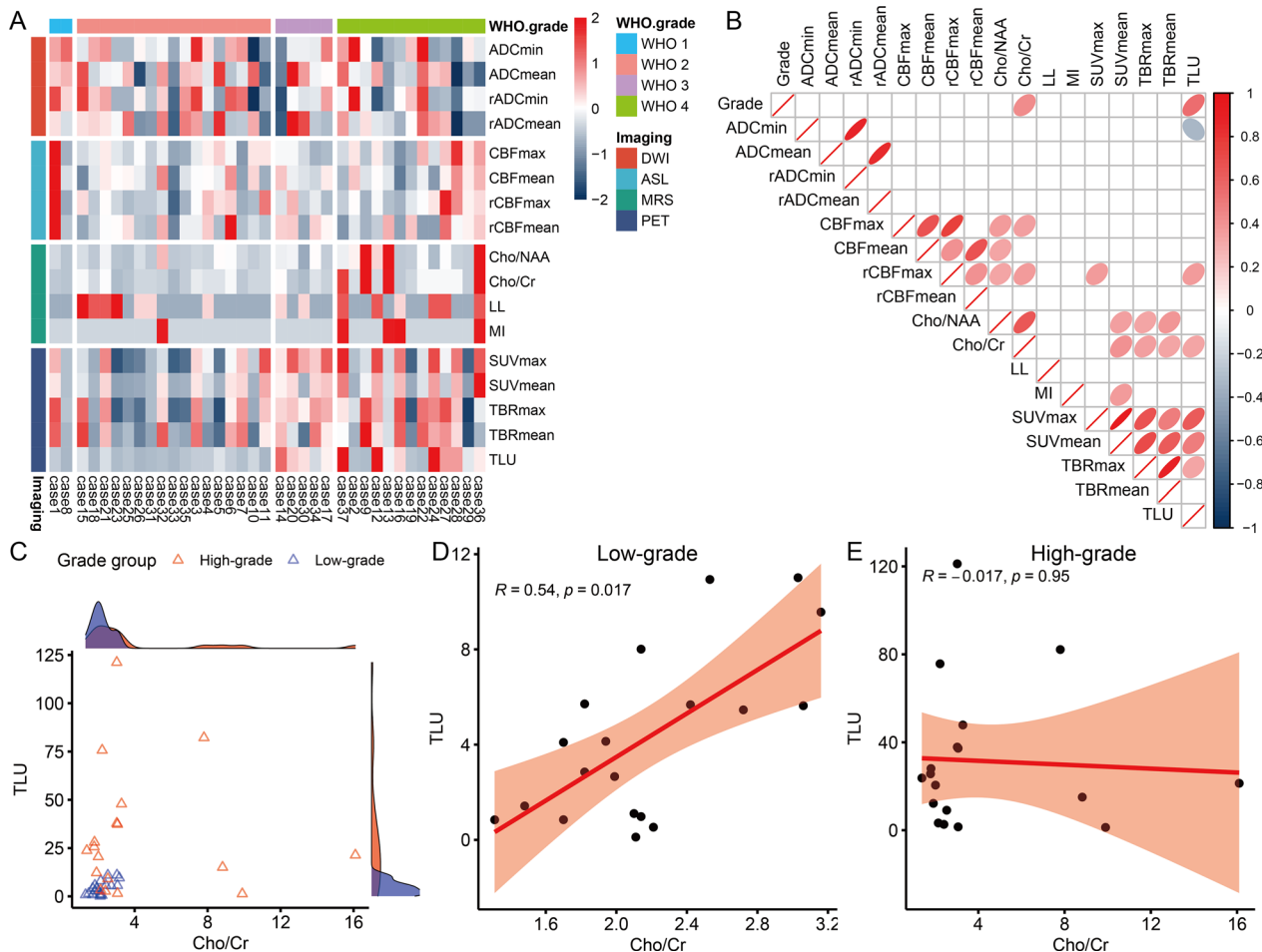


Fig. 6 Correlation between advanced MRI parameters and WHO grades in PET-negative gliomas. **A** Heatmap of Z-score based on multiparametric MRI classified by WHO grade. **B** Heatmap of correlation between advanced MRI parameter and WHO grade. The WHO grade correlated with Cho/Cr and TLU ($r = 0.43$ and 0.55 ; $p = 0.007$ and < 0.001 ; respectively). And there was a correlation between Cho/Cr and TLU ($r = 0.33$, $p = 0.042$). Right skewed (red) ellipse represents positive correlation, and left sloping (blue) ellipse represents negative correlation. Blank squares represent no statistical correlation ($p > 0.05$). **C** Different distribution of TLU and Cho/Cr between high- and low-grade PET-negative gliomas. **D** Scatter plot showing moderated correlation between TLU and Cho/Cr in low-grade PET-negative gliomas ($r = 0.54$, $p = 0.017$). **E** Scatter plot showing no correlation between TLU and Cho/Cr in high-grade PET-negative gliomas ($r = -0.017$, $p = 0.95$). ADC indicates apparent diffusion coefficient; CBF, cerebral blood perfusion; Cho/Cr, choline to creatine; Cho/NAA, choline to acetylaspartate; SUV, standardized uptake value; TLU, total lesion tracer standardized uptake

analysis confirmed that ADC values of PET-negative gliomas exhibiting lower tumor cell density activity were not correlated with WHO grades. Thus, the ADC parameters cannot be used for diagnosing PET-negative glioma grading or differentiating PET-negative gliomas from

other lesions. Although ADC_{min} and $rADC_{min}$ were not different between PET-negative gliomas and non-glioma lesions, the relative ADC values of PET-negative gliomas and non-glioma lesions were more than one. And numerous studies have similarly reported that low-grade

gliomas exhibit $rADC_{\min}$ values greater than one, with astrocytomas in particular having higher $rADC_{\min}$ [12, 37, 38].

The ability of CBF parameters to discriminate gliomas from other cerebral lesions is controversial in many studies. Partial studies found that neoplastic lesions had a higher CBF than those of non-neoplastic lesions, and the CBF of glioblastomas was significantly higher than that of metastasis [18, 39]. Nevertheless, other studies demonstrated that non-neoplastic cerebral lesions may show increased perfusion in CBF map similar to high-grade gliomas [40]. We also found no statistically significant difference in CBF parameters between PET-negative gliomas and non-glioma lesions. A possible explanation for this might be that PET-negative gliomas have a lower cell density, resulting in a reduced requirement for cerebral blood flow supply. This could explain why the CBF parameters used in this study were unable to distinguish the gliomas from other cerebral lesions. And previous studies confirmed that CBF parameters of gliomas were associated with grades [41–43]. However, the correlation between CBF and grades was not observed in the PET-negative gliomas. This result may be explained by the fact that 2021 WHO grade of gliomas is more dependent on molecular markers. Therefore, the degree of amino acid uptake in PET-negative gliomas may not be correlated with the updated tumor grade. Vettermann et al. [25] also thought WHO grade may not affect the uptake of glioma $[^{18}\text{F}]\text{FET}$ mediated by LAT1, and they proposed the hypothesis that there are unknown biological processes affecting glioma $[^{18}\text{F}]\text{FET}$ uptake.

The single most striking marked observation to emerge from the data comparison was that the Cho/NAA and Cho/Cr of PET-negative gliomas were higher than those of non-gliomas, and Cho/Cr was an independent risk factor for identifying PET-negative gliomas in this study. These results were similar to those of Ikeguchiet al. [16] who also found that the Cho/NAA ratio was significantly higher in gliomas than in demyelination. Some studies also supported our findings that Cho/Cr of gliomas were higher than that of metastasis [44]. This result could be attributed to the stronger invasions of tumor cells in gliomas, which leads to a higher degree of local tumor cell infiltration compared to other cerebral tumors [17]. The Cho/Cr ratio indicates the metabolic activity of tumor cell membranes, which correlates with tumor proliferation and invasion. Consequently, within a single voxel, gliomas contain a greater proportion of indistinct margins (indicative of invasion) and tumor core, resulting in a higher Cho/Cr ratio compared to metastatic tumors and demyelinating lesions. And correlation analysis revealed a simultaneous correlation between Cho/Cr measured

by MRS and TLU measured by PET, with WHO grades in PET-negative gliomas. Moreover, different correlation between TLU and Cho/Cr supported that MRS could identify PET-negative gliomas and provide potentially clues for subsequent studies on the mechanisms of low $[^{18}\text{F}]\text{FET}$ uptake in gliomas. In light of the previous finding by Vettermann et al. [25], it could conceivably be explained as that certain mechanisms associated with tumor grading or molecular typing have the potential to interfere with the transport of FET by LAT proteins of PET-negative gliomas while not affecting the changes of Cho/Cr in gliomas. Therefore, the multiparametric MRI nomogram that combined the T2-FLAIR mismatch sign and Cho/Cr performed best in identifying PET-negative gliomas.

We acknowledge that our research possesses three limitations. Firstly, constrained by the smaller sample size of PET-negative isolated cerebral lesions, the non-glioma lesions analyzed in this study consisted mainly of demyelination and brain metastasis. There is a need for future studies to explore the value of multi-parametric MRI for identifying PET-negative lymphomas, brain abscesses, and other cerebral lesions. Secondly, although an integrated PET/MR scanner was used to investigate the correlation between multiparametric MRI and PET-negative isolated cerebral lesions, it is necessary to use PET/CT and MR for further validation. Thirdly, the hotspot areas based on 2D MRS scanning may differ from the hotspot areas of ADC or CBF maps. This may have imparted a limitation to the ADC and CBF parameters, preventing them from offering supplementary diagnostic value when combined with MRS parameters. The 3D MRS scanning in the future has the potential to further improve the diagnostic utility of multi-parametric MRI.

Conclusions

An approach combining the T2-FLAIR mismatch sign and Cho/Cr can enhance the identification of $[^{18}\text{F}]\text{FET}$ PET-negative gliomas to better apply multiparametric MRI in the diagnosis and surgical decision of $[^{18}\text{F}]\text{FET}$ PET-negative gliomas. Moreover, the correlation between $[^{18}\text{F}]\text{FET}$ uptake and Cho/Cr affected by the new version of tumor grading related to molecular subtyping can support further research into the mechanisms of reduced $[^{18}\text{F}]\text{FET}$ uptake in gliomas.

Abbreviations

ADC _{min}	Minimal apparent diffusion coefficient
ASL	Arterial spin labeling
AUC	Area under the receiver operating characteristic curve
CBF	Cerebral blood perfusion
Cho/Cr	Choline to creatine
Cho/NAA	Choline to acetylaspartate

DCA	Decision curve analysis
DWI	Diffusion-weighted imaging
[¹⁸ F]FET	[¹⁸ F]fluoroethyl-L-tyrosine
IDHmut-Noncode1	IDH-mutant with 1p/19q non-codeleted
LL	Lactate-lipid
MI	Myo-inositol
MRS	Magnetic resonance spectroscopy
NRI	Net reclassification improvement
PET	Positron emission tomography
OR	Odds Ratio
rADC _{min}	Relative minimal apparent diffusion coefficient
rCBF _{max}	Relative maximum cerebral blood perfusion
ROC	Receiver operating characteristic curve
SD	Standard deviation
SUV _{max}	Maximum standardized uptake value
SUV _{mean}	Mean standardized uptake value
TBR _{max}	Maximal tumor to background ratio
TLU	Total lesion tracer standardized uptake
TV	Tumor volume
T1WI	T1 weighted imaging
T1CE	T1 contrast enhanced
T2-FLAIR	T2 fluid attenuated inversion recovery
T2WI	T2 weighted imaging
CNS tumors WHO classification	World Health Organization classification of tumors of the central nervous system taxonomy

Supplementary Information

The online version contains supplementary material available at <https://doi.org/10.1186/s13550-025-01224-8>.

Additional file 1.

Additional file 2.

Additional file 3.

Acknowledgements

Thanks to Dr. Hongwei Yang, Dr. Lei Ma, and Dr. Yu Yang for their support of data acquisition in this study.

Author contributions

JL, XRX, and XRL performed the conceptualization and study design. XRL, YC, XH, and BXC performed data curation, investigation, and formal analysis; MZ analyzed the pathology. HUL supplied the support of the methodology and visualization. JL provided resources, funding, and project administration. XRL and BXC performed the validation. XRL and XRX wrote the original draft. All authors have participated in critical revision and writing of the article. All authors have read and agreed to the published version of the manuscript.

Funding

This research has been supported in part by the National Key Research and Development Program of China (No. 2022YFC2406900), and the Huizhi Ascent Project of Xuanwu Hospital (HZ2021ZCLJ005).

Availability of data and materials

The datasets used during the current study are available from the corresponding author on reasonable request.

Declarations

Ethics approval and consent to participate

The study was performed according to the guidelines of the Declaration of Helsinki and approved by the Xuanwu hospital ethics committee (protocol code: Xuanwu hospital [2023] 044). Written Informed consent was obtained from all patients involved in the study.

Consent for publication

The data presented have been approved for publication and each patient has provided written informed consent.

Competing interests

The authors of this manuscript declare no relationships with any companies, whose products or services may be related to the subject matter of the article.

Author details

¹Department of Radiology and Nuclear Medicine, Xuanwu Hospital, Capital Medical University, Beijing, China. ²Beijing Key Laboratory of Magnetic Resonance Imaging and Brain Informatics, Capital Medical University, Beijing, China. ³Department of Neurosurgery, Xuanwu Hospital, Capital Medical University, Beijing, China. ⁴Department of Pathology, Xuanwu Hospital, Capital Medical University, Beijing, China. ⁵GE Healthcare, Beijing, China.

Received: 28 October 2024 Accepted: 11 March 2025

Published online: 07 April 2025

References

- Albert NL, Galldiks N, Ellingson BM, van den Bent MJ, Chang SM, Cicone F, et al. PET-based response assessment criteria for diffuse gliomas (PET RANO 1.0): a report of the RANO group. *Lancet Oncol*. 2024;25:e29-41.
- Law I, Albert NL, Arbizu J, Boellaard R, Drzezga A, Galldiks N, et al. Joint EANM/EANO/RANO practice guidelines/SNMMI procedure standards for imaging of gliomas using PET with radiolabelled amino acids and [¹⁸F] FDG: version 1.0. *Eur J Nucl Med Mol Imaging*. 2019;46:540-57.
- Weller M, van den Bent M, Tonn JC, Stupp R, Preusser M, Cohen-Jonathan-Moyal E, et al. European Association for Neuro-Oncology (EANO) guideline on the diagnosis and treatment of adult astrocytic and oligodendroglial gliomas. *Lancet Oncol*. 2017;18:E315-29.
- Albert NL, Winkelmann I, Suchorska B, Wenter V, Schmid-Tannwald C, Mille E, et al. Early static (18)F-FET-PET scans have a higher accuracy for glioma grading than the standard 20-40 min scans. *Eur J Nucl Med Mol Imaging*. 2016;43:1105-14.
- Lohmann P, Herzog H, Rota Kops E, Stoffels G, Judov N, Filss C, et al. Dual-time-point O-(2-[¹⁸F]fluoroethyl)-L-tyrosine PET for grading of cerebral gliomas. *Eur Radiol*. 2015;25:3017-24.
- Kertels O, Kessler AF, Mihovilovic M, Stolzenburg A, Linsenmann T, Samnick S, et al. Prognostic value of O-(2-[¹⁸F]fluoroethyl)-L-tyrosine PET/CT in newly diagnosed WHO 2016 Grade II and III Glioma. *Mol Imaging Biol*. 2019;21:1174-81.
- Hangel G, Schmitz-Abecassis B, Sollmann N, Pinto J, Arzanforoosh F, Barkhof F, et al. Advanced MR techniques for preoperative glioma characterization: part 2. *J Magn Reson Imaging*. 2023;57:1676-95.
- Johnson DR, Giannini C, Vaubel RA, Morris JM, Eckel LJ, Kaufmann TJ, et al. A radiologist's guide to the 2021 WHO central nervous system tumor classification: part I-key concepts and the spectrum of diffuse gliomas. *Radiology*. 2022;304:494-508.
- Jain R, Johnson DR, Patel SH, Castillo M, Smits M, van den Bent MJ, et al. "Real world" use of a highly reliable imaging sign: "T2-FLAIR mismatch" for identification of IDH mutant astrocytomas. *Neuro Oncol*. 2020;22:936-43.
- Mabray MC, Cohen BA, Villanueva-Meyer JE, Valles FE, Barajas RF, Rubenstein JL, et al. Performance of apparent diffusion coefficient values and conventional MRI features in differentiating tumefactive demyelinating lesions from primary brain neoplasms. *Am J Roentgenol*. 2015;205:1075-85.
- Xiao X, Liu X, Liang W, Han L-Y, Li X-D, Guo L-J, et al. Conventional MRI features of central nervous system embryonal tumor, not otherwise specified in adults: comparison with glioblastoma. *Acad Radiol*. 2022;29:S44-51.
- Zhang S, Wang J, Wang K, Li X, Zhao X, Chen Q, et al. Differentiation of high-grade glioma and primary central nervous system lymphoma: multiparametric imaging of the enhancing tumor and peritumoral regions based on hybrid F-18-FDG PET/MRI. *Eur J Radiol*. 2022;150: 110235.
- Hirschler L, Sollmann N, Schmitz-Abecassis B, Pinto J, Arzanforoosh F, Barkhof F, et al. Advanced MR techniques for preoperative glioma characterization: part 1. *J Magn Reson Imaging*. 2023;57:1655-75.

14. Ozturk-Isik E, Cengiz S, Ozcan A, Yakicier C, Ersen Danyeli A, Pamir MN, et al. Identification of *IDH* and *TERTp* mutation status using ¹H-MRS in 112 hemispheric diffuse gliomas. *J Magn Reson Imaging*. 2020;51:1799–809.
15. Su X, Yang X, Sun H, Liu Y, Chen N, Li S, et al. Evaluation of key molecular markers in adult diffuse gliomas based on a novel combination of diffusion and perfusion MRI and MR spectroscopy. *J Magn Reson Imaging*. 2024;59(2):628–38. <https://doi.org/10.1002/jmri.28793>.
16. Ikeguchi R, Shimizu Y, Abe K, Shimizu S, Maruyama T, Nitta M, et al. Proton magnetic resonance spectroscopy differentiates tumefactive demyelinating lesions from gliomas. *Multiple Scler Relat Disord*. 2018;26:77–84.
17. Weinberg BD, Kuruva M, Shim H, Mullins ME. Clinical applications of magnetic resonance spectroscopy in brain tumors. *Radiol Clin N Am*. 2021;59:349–62.
18. Hu W, Guo F, Xu Y, Xi Y, He B, Yin H, et al. Differentiation of neoplastic and non-neoplastic intracranial enhancement lesions using three-dimensional pseudo-continuous arterial spin labeling. *Front Neurosci*. 2022;16:812997.
19. Sawlani V, Patel MD, Davies N, Flintham R, Wesolowski R, Ughratdar I, et al. Multiparametric MRI: practical approach and pictorial review of a useful tool in the evaluation of brain tumours and tumour-like lesions. *Insights Imaging*. 2020;11:84.
20. Makino K, Hirai T, Nakamura H, Kuroda J, Shinojima N, Uetani H, et al. Differentiating between primary central nervous system lymphomas and glioblastomas: combined use of perfusion-weighted and diffusion-weighted magnetic resonance imaging. *World Neurosurg*. 2018;112:E1–6.
21. Haubold J, Demircioglu A, Gratz M, Glas M, Wrede K, Sure U, et al. Non-invasive tumor decoding and phenotyping of cerebral gliomas utilizing multiparametric 18F-FET PET-MRI and MR fingerprinting. *Eur J Nucl Med Mol Imaging*. 2020;47:1435–45.
22. Verburg N, Koopman T, Yaqub MM, Hoekstra OS, Lammertsma AA, Barkhof F, et al. Improved detection of diffuse glioma infiltration with imaging combinations: a diagnostic accuracy study. *Neuro Oncol*. 2020;22:412–22.
23. Harat M, Rakowska J, Harat M, Szyllberg T, Furtak J, Miechowicz I, et al. Combining amino acid PET and MRI imaging increases accuracy to define malignant areas in adult glioma. *Nat Commun*. 2023;14:4572.
24. Pyka T, Krzyzanowska I, Rominger A, Delbridge C, Meyer B, Boeckh-Behrens T, et al. Multiparametric characterization of intracranial gliomas using dynamic [18F]FET-PET and magnetic resonance spectroscopy. *Diagnostics (Basel)*. 2022;12:2331.
25. Vettermann FJ, Diekmann C, Weidner L, Unterrainer M, Suchorska B, Ruf V, et al. L-type amino acid transporter (LAT) 1 expression in F-18-FET-negative gliomas. *EJNMMI Res*. 2021;11:124.
26. Piccardo A, Tortora D, Mascelli S, Severino M, Piatelli G, Consales A, et al. Advanced MR imaging and F-18-DOPA PET characteristics of H3K27M-mutant and wild-type pediatric diffuse midline gliomas. *Eur J Nucl Med Mol Imaging*. 2019;46:1685–94.
27. Yamasaki F, Takayasu T, Nosaka R, Amatya VJ, Doskaliyev A, Akiyama Y, et al. Magnetic resonance spectroscopy detection of high lipid levels in intraaxial tumors without central necrosis: a characteristic of malignant lymphoma. *JNS*. 2015;122:1370–9.
28. Von Rohr K, Unterrainer M, Holzgreve A, Kirchner MA, Li Z, Unterrainer LM, et al. Can radiomics provide additional information in [(18)F]FET-negative gliomas? *Cancers*. 2022;14:4860.
29. Louis DN, Perry A, Wesseling P, Brat DJ, Cree IA, Figarella-Branger D, et al. The 2021 WHO classification of tumors of the central nervous system: a summary. *Neuro Oncol*. 2021;23:1231–51.
30. Hiremath SB, Muraliedharan A, Kumar S, Nagesh C, Kesavadas C, Abraham M, et al. Combining diffusion tensor metrics and DSC perfusion imaging: can it improve the diagnostic accuracy in differentiating tumefactive demyelination from high-grade glioma? *Am J Neuroradiol*. 2017;38:685–90.
31. Kang KM, Song J, Choi Y, Park C, Park JE, Kim HS, et al. MRI scoring systems for predicting isocitrate dehydrogenase mutation and chromosome 1p/19q codeletion in adult-type diffuse glioma lacking contrast enhancement. *Radiology*. 2024;311: e233120.
32. Ding Y, Xing Z, Liu B, Lin X, Cao D. Differentiation of primary central nervous system lymphoma from high-grade glioma and brain metastases using susceptibility-weighted imaging. *Brain Behav*. 2014;4:841–9.
33. Jekel L, Brim WR, von Reppert M, Staib L, Petersen GC, Merkaj S, et al. Machine learning applications for differentiation of glioma from brain metastasis—a systematic review. *Cancers*. 2022;14:1369.
34. Caravan I, Ciortea CA, Contis A, Lebovici A. Diagnostic value of apparent diffusion coefficient in differentiating between high-grade gliomas and brain metastases. *Acta Radiol*. 2018;59:599–605.
35. Mouthuy N, Cosnard G, Abarca-Quinones J, Michoux N. Multiparametric magnetic resonance imaging to differentiate high-grade gliomas and brain metastases. *J Neuroradiol*. 2012;39:301–7.
36. Ponisio MR, McConathy JE, Dahiya SM, Miller-Thomas MM, Rich KM, Salter A, et al. Dynamic 18F-FDOPA-PET/MRI for the preoperative evaluation of gliomas: correlation with stereotactic histopathology. *Neurooncol Pract*. 2020;7:656–67.
37. Li M, Ren X, Chen X, Wang J, Shen S, Jiang H, et al. Combining hyperintense FLAIR rim and radiological features in identifying IDH mutant 1p/19q non-codeleted lower-grade glioma. *Eur Radiol*. 2022;32:3869–79.
38. Morana G, Piccardo A, Tortora D, Puntoni M, Severino M, Nozza P, et al. Grading and outcome prediction of pediatric diffuse astrocytic tumors with diffusion and arterial spin labeling perfusion MRI in comparison with 18F-DOPA PET. *Eur J Nucl Med Mol Imaging*. 2017;44:2084–93.
39. Weber MA, Zoubaa S, Schlieter M, Juettler E, Huttner HB, Geletnek K, et al. Diagnostic performance of spectroscopic and perfusion MRI for distinction of brain tumors. *Neurology*. 2006;66:1899–906.
40. Barbosa BC, Marchiori E, Leal Leidersneider C, Brandao L, Castillo M. Demyelinating lesions behaving like aggressive tumours on advanced MRI techniques. *Neuroradiol J*. 2019;32:103–7.
41. Cebeci H, Aydin O, Ozturk-Isik E, Gumus C, Inecikli F, Bekar A, et al. Assessment of perfusion in glial tumors with arterial spin labeling; comparison with dynamic susceptibility contrast method. *Eur J Radiol*. 2014;83:1914–9.
42. Delgado AF, De Luca F, van Westen D, Delgado AF. Arterial spin labeling MR imaging for differentiation between high- and low-grade glioma: a meta-analysis. *Neuro Oncol*. 2018;20:1450–61.
43. Shen N, Zhao L, Jiang J, Jiang R, Su C, Zhang S, et al. Intravoxel incoherent motion diffusion-weighted imaging analysis of diffusion and microperfusion in grading gliomas and comparison with arterial spin labeling for evaluation of tumor perfusion. *J Magn Reson Imaging*. 2016;44:620–32.
44. Ankush A, Sardesai S. Role of MRSI major metabolite ratios in differentiating between intracerebral ring-enhancing neoplastic and non-neoplastic lesions, high-grade gliomas and metastases, and high-grade and low-grade gliomas. *Cureus*. 2022;14: e31841.

Publisher's Note

Springer Nature remains neutral with regard to jurisdictional claims in published maps and institutional affiliations.